Fizika Nizkikh Temperatur, 2008, v. 34, No. 10, p. 942–946

Magnetic proximity effect in $La_{0.7}Ca_{0.3}MnO_3/La_{0.9}Ca_{0.1}MnO_3$ multilayered film with diffusive interfaces

V.G. Prokhorov and G.G. Kaminsky

Institute of Metal Physics, National Academy of Sciences of Ukraine, Kiev 03142, Ukraine
E-mail: pvg@imp.kiev.ua

Y.P. Lee, S.Y. Park, Y.H. Hyun, and J.S. Park

q-Psi and Department of Physics, Hanyang University, Seoul, 133-791, Korea

V.L. Svetchnikov

National Center for HREM, TU Delft, 2628AL, The Netherlands

Received April 2, 2008

The structural, the magnetic and the transport properties of $La_{0.7}Ca_{0.3}MnO_3/La_{0.9}Ca_{0.1}MnO_3$ multilayer film, prepared by rf-magnetron sputtering, have been investigated. The high-resolution electron-microscopy studies reveal the formation of different crystal structures in the constituent sublayers, but without sharp and well-defined interfaces. At the same time, the small regions of double-period modulated phase exist in the $La_{0.9}Ca_{0.1}MnO_3$ sublayers at room temperature, manifesting the formation of charge-ordered antiferromagnetic state. The magnetic measurements reveal a significant enhancement of the ferromagnetic ordering in the $La_{0.9}Ca_{0.1}MnO_3$ layers due to a strong magnetic coupling between the constituent sublayers. The multilayer film shows the anisotropic saturation magnetization at low temperature and the alternating shape of the temperature-dependent anisotropic magnetoresistance near the metal–insulator transition.

PACS: **71.30.+h** Metal–insulator transitions and other electronic transitions;
75.47.Gk Colossal magnetoresistance;
75.47.Lx Manganites.

Keywords: manganite, multilayered film, diffusive interface, magnetic proximity effect.

1. Introduction

The hole-doped perovskite manganites continue to attract intense theoretical and experimental attention because of not only their interesting fundamental science, connected with the discovery of colossal magnetoresistance (CMR), but their potential applications to new devices such as magnetic reading heads, field sensors and memories. For a great number of these potential industrial applications, these materials have to be prepared in the form of thin films or multilayered hybrid systems. However, thin manganite films frequently show different magnetotransport properties in compare to bulk materials and the multilayer structure demonstrates the magnetic behavior substantially differ from those for the individual constituent layers. The observed discrepancy is mainly explained by an accumulation of the lattice strain, due to the epitaxial growth of the film, which plays an important role in a formation of the spin-ordered state and the value of CMR effect [1–10]. This phenomenon is provided by a close relationship between electronic transfer integral, and both Mn–O bond length and Mn–O–Mn angle [11], and is described, as a rule, on the base of Millis model [12] developed for materials with weak lattice strains and a cubic symmetry. At the same time, it is well-known that the ferromagnetic (FM) ground state in manganites is provided by the Zener double-exchange interaction by means of an electron transfer from Mn^{3+} to Mn^{4+} via oxygen [13]. Since any plane structural defect blocks up the electron motion, the FM coupling between the adjacent sublayers in a multilayer structure will be greatly depend on the interface origin. It was shown recently that the FM coupling between sublayers (magnetic proximity effect) is observed in the manganite multilayer films with a coherent (diffusive) interfaces only [14]. In the case of an incoherent interface, which is formed by the misfit

dislocations, multilayer film manifests the simple superposition of the magnetic properties, which are typical for the individual sublayers.

In this paper, we report the experimental results for $La_{0.7}Ca_{0.3}MnO_3/La_{0.9}Ca_{0.1}MnO_3$ multilayer (ML) film with the diffusive interface between sublayers, emphasizing a significant enhancement of the FM ordering in the ultrathin $La_{0.9}Ca_{0.1}MnO_3$ layers with an origin for the magnetic and magnetoresistance anisotropy, which are explained by the magnetic proximity effect.

2. Experimental techniques

All the films were prepared by rf-magnetron sputtering using the so-called «soft» (or powder) target [15]. The substrate was a $LaAlO_3$ (001) single crystal (LAO) with an out-of-plane lattice parameter $\simeq$ 0.379 nm for the pseudocubic symmetry. The substrate temperature during deposition was 720 °C. The ML film contains five $La_{0.7}Ca_{0.3}MnO_3$ (LCM1) and five $La_{0.9}Ca_{0.1}MnO_3$ (LCM2) sublayers with LCM1 at the top. The thickness of all the sublayers was 10 nm. For comparison the bare LCM1 and LCM2 films with a thickness of 100 nm were also prepared at the same conditions. The θ–2θ x-ray diffraction (XRD) patterns were obtained using a Rigaku diffractometer with Cu K_α radiation. The lattice parameters evaluated directly from the XRD data were plotted against $\cos^2\theta/\sin\theta$. From the intercept of the extrapolated straight line to $\cos^2\theta/\sin\theta = 0$, a more precise lattice parameter was obtained. The high-resolution electron-microscopy (HREM) study was carried out using a Philips CM300UT-FEG microscope with a field emission gun operated at 300 kV. The point resolution of the microscope was in the order of 0.12 nm. The cross-sectional specimens were prepared by the standard techniques using mechanical polishing followed by ion-beam milling at a grazing incidence. All microstructure measurements were taken at a room temperature. The resistance measurements were carried out by using the four-probe method in a temperature range of 4.2–300 K and a magnetic field up to 5 T. The field-cooled (FC) and the zero-field-cooled (ZFC) magnetization curves were taken with a Quantum Design SQUID magnetometer.

3. Microstructure

Figure 1,*a* shows the θ–2θ XRD scan for the ML film. The (00*l*) Bragg peaks of high intensity for the film (denoted by ML) and the substrate (denoted by LAO) are observed only, indicating that the deposition results in the highly *c*-oriented crystal structure. At the same time, the inset exhibits that the (002) Bragg peak for ML is slightly splitted, manifesting the presence of the two different crystalline phases. The (002) Bragg peaks, corresponding to the bare LCM1 and LCM2 films, are shown for comparison, as well. The high-

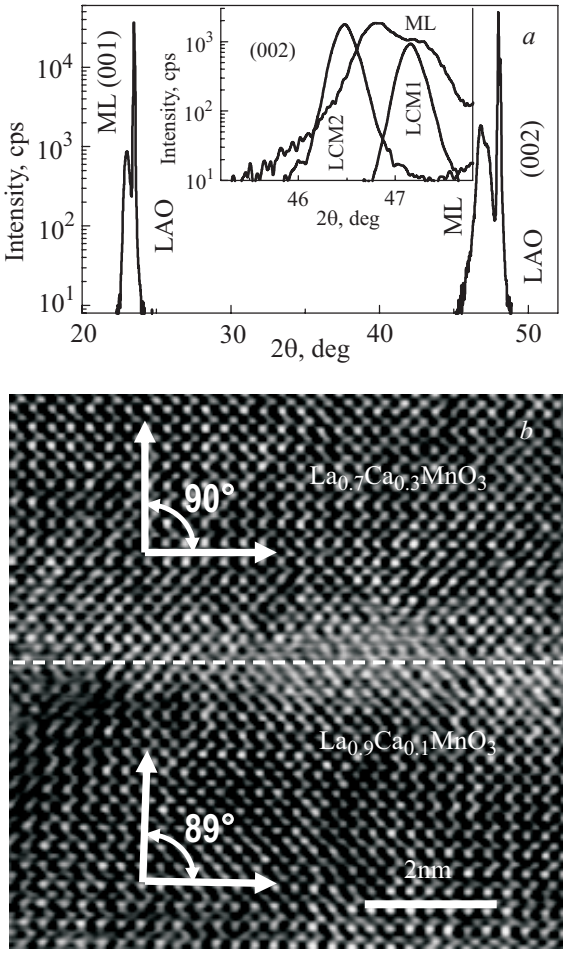

Fig. 1. (*a*) The θ–2θ XRD scan for the ML film. ML and LAO denote the Bragg peaks, corresponding to the film and substrate, respectively. Inset exhibits the (002) Bragg peak for ML, LCM1 and LCM2 in detail. (*b*) High-magnification cross-sectional HREM image of the ML film. Dashed line indicates the interface between sublayers.

magnification cross-sectional HREM image for the ML film, represented by Fig. 1,*b*, reveals a formation of different crystal structure in the two constituent sublayers (orthorhombic, with a right angle between the atomic rows, and rhombohedral, with the corresponding angle about 89°, for LCM1 and LCM2, respectively), but without sharp and well-defined interface between sublayers (denoted by dashed line). A formation of diffusive interfaces is explained by the relatively high substrate temperature (720 °C) at deposition of the ML film. Inset in Fig. 2,*a* displays the fast-Fourier-transform (FFT) pattern of the HREM image taken for three layers of the ML film. White arrows indicate a slight splitting of basic Bragg spots, similar to observed on the XRD scan, manifesting the presence of sublayers with different crystal lattice. At the same time, the small regions of double-period modulated phase exist in the LCM2 sublayers at room temperature (see Fig. 2,*b*). In this case the FFT of HREM image, represented by Fig. 2,*c*, produces not only a rectangular pattern of the basic Bragg spots, which are typical for a

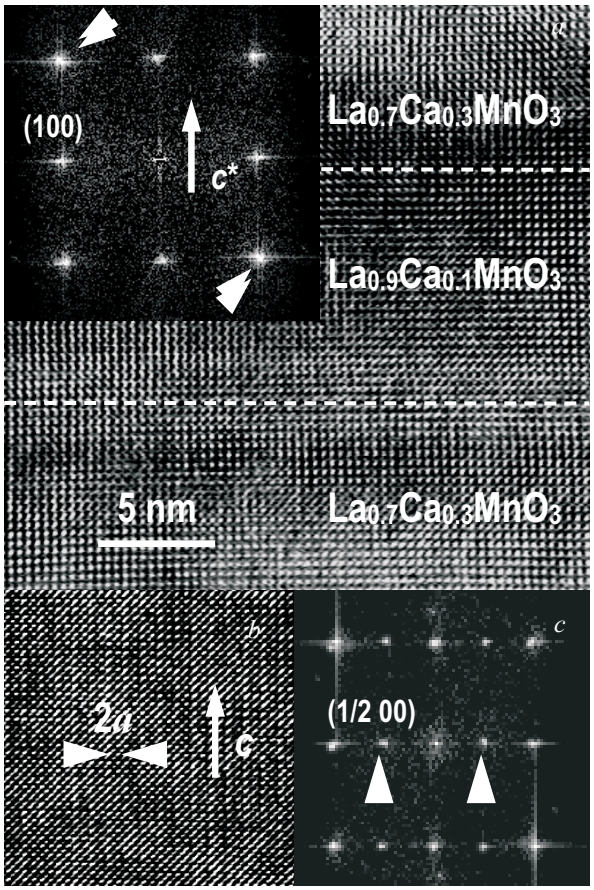

Fig. 2. (*a*) High-magnification cross-sectional HREM image of the ML film. Dashed lines indicate the interface between sublayers. Inset is the corresponding FFT of this HREM image. White arrows indicate the splitting of fundamental Bragg spots, manifesting the presence of two different crystal lattices. (*b*) Selected area in the LCM2 sublayer demonstrates a modulated stripe structure with the doubled *a*-axis lattice period. (*c*) The corresponding FFT of this HREM image. White arrows indicate the superlattice spots.

regular pseudocubic crystal lattice, but additional superlattice reflections with a wave vector $q = a^*/2$ (indicated by white arrows), where a^* is the reciprocal lattice vector along the *a* axis of the simple pseudocubic symmetry. The similar superlattice spots in FFT pattern were already observed for the $La_{0.5}Ca_{0.5}MnO_3$ film and treated as appearance of a charge ordering of Mn^{4+} and Mn^{3+} ions [16]. Like the half-doped $La_{0.5}Ca_{0.5}MnO_3$ film, there is no sharp boundary between modulated and unmodulated (charge-disordered) regions. Instead, one phase is blended gradually with the other. This phase does not exceed any percents of the film volume and occupies the areas closed to the substrate. An appearance of the charge-ordered state in ultrathin manganite films is explained by a nonuniform distribution of the lattice strain due to an epitaxial growth mode.

Therefore, ML can be treated as a continuous film without sharp interfaces between sublayers, while with a long-range modulation of the crystal lattice along the *c* axis.

4. Magnetic and transport properties

Figure 3,*a* shows the in-plane ZFC and FC temperature-dependent magnetization curves for the bare LCM1 (*1*) and LCM2 (*2*), and the ML (*3*) films. Arrows denote the corresponding Curie temperatures (T_C). The bare LCM1 film undergoes a sharp transition to the FM state at T_C = = 230 K, while the bare LCM2 demonstrates the FM ordering at $T_C \simeq 155$ K, followed by a partial transition to the antiferromagnetic (AFM) state with decreasing temperature (curves *2* in Fig. 3,*a*). The obtained T_C values are

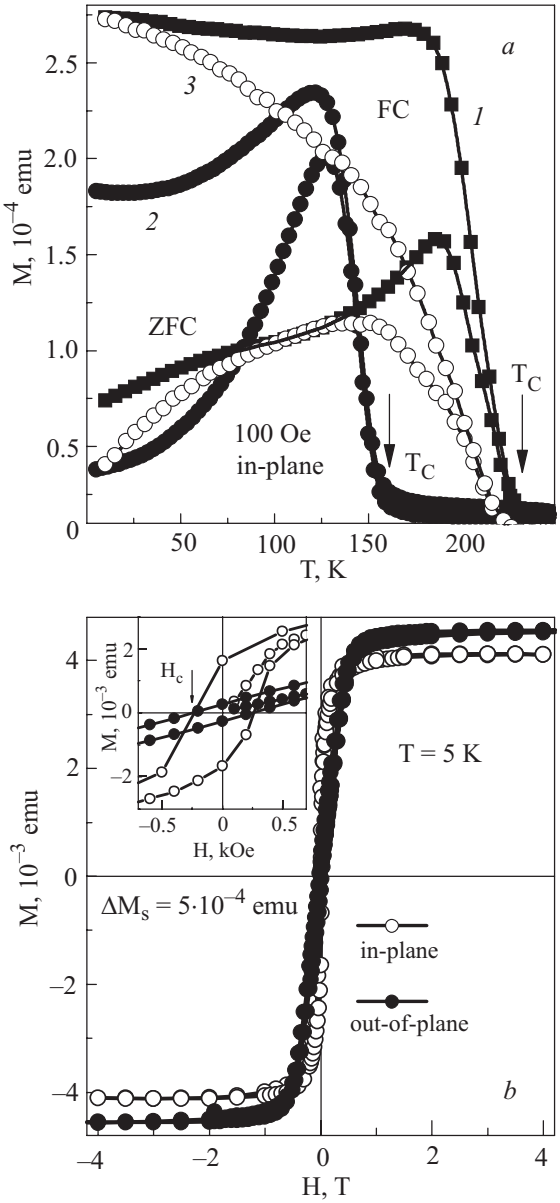

Fig. 3. (*a*) Temperature dependence of the ZFC and the FC magnetization for LCM1 (*1*), LCM2 (*2*) and ML (*3*) at an in-plane applied magnetic field of 100 Oe. Arrows indicate the Curie points. Lines are guides to the eyes. (*b*) In-plane (open symbols) and out-of-plane (solid symbols) hysteresis loops for ML at temperature of 5 K. Inset is the same curves in low-field range. H_c is coersive magnetic field. Lines are guides to the eyes.

almost coincident with that for the bulk compounds: T_C = = 265 and 160 K for $La_{0.7}Ca_{0.3}MnO_3$ and $La_{0.9}Ca_{0.1}MnO_3$ [17,18], respectively. The observed slight decrease of T_C is typical for thin manganite films and is explained by an influence of the lattice strain [12]. However, even though a half of the volume of ML film consists of the LCM2 sublayers with a low Curie point and the low-temperature AFM state, the ML film manifests only single-phase FM transition at $T_C \simeq 230$ K. At the same time, this transition is very broad in comparison with bare the LCM1 and the LCM2 films and the magnetization becomes saturated only at lowest temperature. Such kind of the FC $M(T)$ behavior is typical for an inhomogeneous magnetic system. In principal, the ML film can be treated as an artificially-formed inhomogeneous system that consist of five FM sublayers with $T_C = 230$ K (LCM1) and five FM (AFM) sublayers with $T_C(T_N) = 155$ K (LCM2). In this case, taking the direct summation of the magnetic moments of the separated sublayers, the two-step FC $M(T)$ dependence should be expected. However, in fact, the ML film manifests the smooth averaged FC $M(T)$ curve in the whole temperature range, that can be explained by the induced magnetization in the LCM2 sublayers, due to a magnetic proximity effect. Such magnetic proximity effect can occurs due to the interaction between two magnetic layers with different ordering temperatures. The layer with the higher ordering temperature induces magnetic order into the layer with the lower ordering temperature at temperature at which the latter would be paramagnetic.

An occurrence of the magnetic proximity effect in the ML film is confirmed by the anisotropic behavior of a hysteresis loop, represented by the Fig. 3,*b*. It is seen that the out-of-plane saturation magnetization (M_s) is about ten percents greater than that for the in-plane one. Taking into account, that the magnetic proximity effect does not change the total volume of the FM phase in the ML film (only the ordering temperature can be changed), one can conclude that the observed increase in out-of-plane M_s is connected with the modification of the AFM state in the LCM2 sublayers. It was shown recently, that the mutual interaction between FM and AFM layers can lead to formation of the uncompensated spin state in the AFM phase perpendicular to the film plane, while the in-plane spin component remains compensated [19]. Therefore, it is reasonable to suggest that, due to the proximity effect, the AFM phase of LCM2 transforms in the canted AFM state along out-of-plane direction, which introduces an additional contribution in the out-of-plane M_s value. Inset shows the low-field range of the hysteresis loops in detail. The large difference in the slope between the out-of-plane and in-plane $M(H)$ curves is caused by a demagnetizing factor.

Figure 4 displays the temperature dependence of resistance, $R(T)$, for the LCM1 (*1*), the LCM2 (*2*) and the ML (*3*) films without (solid symbols) and with (open symbols) an applied magnetic field of 5 T. The magnetic field was parallel to the film surface. It is seen that the LCM1 and the ML films manifest the metal–insulator (MI) transitions at the same temperature, $T_P \simeq 225$ K. The LCM3 film shows only a tiny kink-like peculiarity at $T_P \simeq 150$ K. Inset *a* in Fig. 4 presents the temperature dependence of magnetoresistance ratio (MR) for these samples. The MR value is defined by $100\% \times [R(0) - R(H)]/R(H)$, where $R(0)$ and $R(H)$ are the resistances without and with a magnetic field of 5 T, respectively. It is seen that the MR(T) dependence for LCM1 (solid symbols, curve *1*) and ML (open symbols, curve *3*) are practically coincident, while LCM2 (curve *2*) demonstrates the MR effect of a weaker intensity at a lower temperature. Inset *b* in Fig. 4 exhibits the anisotropic MR (AMR) effect for ML, which is not observed for the bare LCM1 and LCM2 films. Here, AMR = $MR_{in\text{-}plane} - MR_{out\text{-}of\text{-}plane}$ is difference between MRs measured at in-plane and out-of-plane applied magnetic field of 5 T. In contrast to the usual anisotropic MR effect, which is observed in the epitaxial manganite films and is manifested as a peak near the MI transition, the ML film reveals an

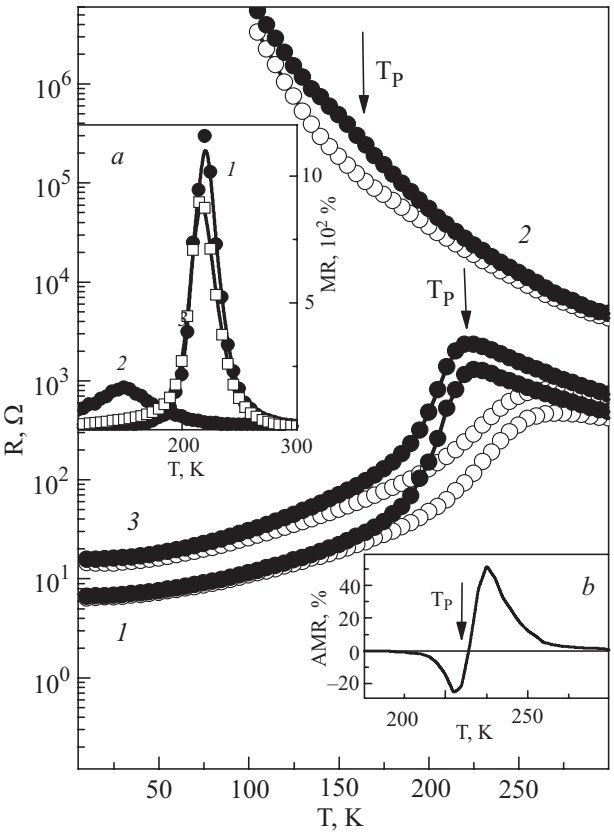

Fig. 4. Temperature dependence of the resistance for LCM1 (*1*), LCM2 (*2*) and ML (*3*) without (solid symbols) and with (open symbols) an applied magnetic field of 5 T. Arrows indicate the temperature of MI transition. Inset *a* displays the temperature-dependent MR ratio for the same films (open symbols correspond to ML). Lines are guides to the eyes. Inset *b* shows temperature dependence of the AMR for ML (see text).

alternating shape of the AMR temperature dependence. This phenomenon can be explained by the competition between the ordinary FM transition in the LCM1 sublayers and the introduced magnetization in the LCM2 ones with decreasing temperature. Figure 3,*b* displays that the out-of-plane M_s value becomes larger than the in-plane one, due to the magnetic proximity effect. Because MR is proportional to square of a magnetization for manganites, the observed alternating AMR(T) behavior is quite expected.

5. Conclusions

The $La_{0.7}Ca_{0.3}MnO_3/La_{0.9}Ca_{0.1}MnO_3$ multilayer film with the diffusive interfaces between constituent sublayers have been prepared by rf-magnetron sputtering at high substrate temperature. In contrast to the ordinary superposition of the magnetic and transport properties of the separated sublayers, the multilayer film demonstrates single-phase ferromagnetic and metal–insulator transition at temperature, which is typical for the bare $La_{0.7}Ca_{0.3}MnO_3$ film. Moreover, the multilayer film manifests the anisotropy of the saturation magnetization at low temperature and the alternating shape of the temperature-dependent anisotropic magnetoresistance near the metal–insulator transition. The observed spin-ordered and magnetoresistance peculiarities are explained by a strong magnetic coupling between constituent sublayers due to a magnetic proximity effect.

Acknowledgments

This work was supported by the KOSEF through the Quantum Photonic Science Research Center and by MOST, Korea. V. Svetchnikov is grateful to the financial support of Netherlands Institute for Metal Research.

1. T.K. Nath, R.A. Rao, D. Lavric, C.B. Eom, L. Wu, and F. Tsui, *Appl. Phys. Lett*. **74**, 1615 (1999).
2. J.R. Sun, C.F. Yeung, K. Zhou, L.Z. Zhou, C.H. Leung, H.K. Wong, and B.G. Shen, *Appl. Phys. Lett*. **76**, 1164 (2000).
3. H.S. Wang, E. Wertz, Y.F. Hu, and Q. Li, *J. Appl. Phys*. **87**, 7409 (2000).
4. R. Desfeux, S. Bailleul, A. Da Costa, W. Prellier, and M. Haghiri-Gosnet, *Appl. Phys. Lett*. **78**, 3681 (2001).
5. A. Biswas, M. Rajeswari, R.C. Srivastava, T. Venkatesan, R.L. Green, Q. Lu, A.L. de Lozanne, and A.J. Millis, *Phys. Rev*. **B63**, 184424 (2001).
6. S. Jacob, T. Roch, F.S. Razavi, G.M. Gross, and H.-U. Habermeier, *J. Appl. Phys*. **91**, 2232 (2002).
7. M. Paranjape, A.K. Raychauhuri, N.M. Mathur, and M.G. Blamire, *Phys. Rev*. **B67**, 2144415 (2003).
8. V.G. Prokhorov, V.A. Komashko, G.G. Kaminsky, V.L. Svetchnikov, H.W. Zandbergen, Y.P. Lee, J.S. Park, and K.W. Kim, *Fiz. Nizk. Temp*. **29**, 161 (2003) [*Low Temp. Phys*. **29**, 117 (2003)].
9. V.G. Prokhorov, G.G. Kaminsky, V.A. Komashko, Y.P. Lee, and J.S. Park, *Fiz. Nizk. Temp*. **29**, 885 (2003) [*Low Temp. Phys*. **29**, 663 (2003)].
10. V.G. Prokhorov, V.A. Komashko, G.G. Kaminsky, K.K. Yu, S.J. Jun, S.Y. Park, J.S. Park, Y.P. Lee, and V.L. Svetchnikov, *Fiz. Nizk. Temp*. **33**, 78 (2007) [*Low Temp. Phys*. **33**, 58 (2007)].
11. H.Y. Hwang, S.W. Cheong, N.P. Ong, and B. Batlogg, *Phys. Rev. Lett*. **77**, 2041 (1996).
12. A.J. Millis, T. Darling, and A. Migliori, *J. Appl. Phys*. **83**, 1588 (1998).
13. C. Zener, *Phys. Rev*. **82**, 403 (1951).
14. V.G. Prokhorov, V.S. Flis, G.G. Kaminsky, and Y.P. Lee, *Fiz. Nizk. Temp*. **30**, 619 (2004) [*Low Temp. Phys*. **30**, 463 (2004)].
15. V.G. Prokhorov, G.G. Kaminsky, V.A. Komashko, J.S. Park, and Y.P. Lee, *J. Appl. Phys*. **90**, 1055 (2001).
16. S.Y. Park, Y.H. Hyun, Y.P. Lee, V.L. Svetchnikov, K.W. Kim, and V.G. Prokhorov, *Appl. Phys. Lett*. **89**, 052502 (2006).
17. Y.H. Li, K.A. Thomas, P.S. de Silva, L.F. Cohen, A. Goyal, M. Rajeswari, N.D. Mathur, M.G. Blamire, J.E. Evetts, T. Venkatesan, and J.L. MacManus-Driscoll, *J. Mater. Res*. **13**, 2161 (1998).
18. P. Schiffer, A.P. Ramirez, W. Bao, and S.-W. Cheong, *Phys. Rev. Lett*. **75**, 3336 (1995).
19. K. Lenz, S. Zander, and W. Kuch, *Phys. Rev. Lett*. **98**, 237201 (2007).